J Mater Sci (2019) 54:2417–2426

Energy materials

Tuning microwave absorption properties of multi-walled carbon nanotubes by surface functional groups

Chenglong Hu[1], Haopeng Liu[1], Yanhui Zhang[1,*], Mu Zhang[1], Jieyi Yu[2], Xianguo Liu[2], and Xuefeng Zhang[1,2,*]

[1] *Key Laboratory for Anisotropy and Texture of Materials (MOE), School of Materials Science and Engineering, Northeastern University, Shenyang 110819, People's Republic of China*

[2] *Innovative Center for Advanced Materials, Hangzhou Dianzi University, Hangzhou 310012, People's Republic of China*

Received: 25 June 2018
Accepted: 4 September 2018
Published online: 30 October 2018

ABSTRACT

Multi-walled carbon nanotubes (MWCNTs) have been proven effective for microwave absorption due to the high dielectric loss capacity; however, the influence of surface functional groups on the absorption efficiency still remains unknown. Herein, we investigated the microwave absorption properties of pristine MWCNTs, hydroxyl-containing MWCNTs and carboxyl-containing MWCNTs, evidencing the absorption efficiencies of $> 33\%$, $> 50\%$ and $> 45\%$ at 8–18 GHz, respectively. Experimental characterizations reveal that the tunability of microwave absorption capacity is originated from the atomic symmetry breaking of surface structure for carbon nanotubes, leading to the differences of electric conductivity and dielectric loss capacity. The present study provides an insight into the structural origin of microwave absorption and has important significance to design microwave absorption materials by chemical surface engineering.

Introduction

The microwave absorbers have been paid much attention and studied extensively due to their wide applications in both commercial and military purposes, such as the avoidance of interference for electronics and the design of invisible aircraft [1–6]. Among all the candidates, ferrites have attracted great interests utilized as microwave absorbers with their large resistivity and magnetic loss [7–12]. However, the applications of these magnetic materials are severely limited by their unavoidable disadvantage of overweight. The required microwave absorbers usually possess lightweight, thin thickness, wideband absorption and thermal stability [13–17].

Since the discovery in 1991 [18], carbon nanotube (CNT) has attracted considerable interest due to its performance of electric conductivity, chemical stability, high aspect ratio and thermal stability [19–21]. Benefiting from the high dielectric characteristics, CNT has exhibited promising potentials for microwave absorption materials with the relatively light density compared with the magnetic components.

Address correspondence to E-mail: yhzhang@mail.neu.edu.cn; zhangxf@atm.neu.edu.cn

https://doi.org/10.1007/s10853-018-2895-y

For example, Che and Liu reported that CNT/crystalline Fe nanocomposites and CNT/zinc oxide whisker composites possess excellent microwave absorption properties [22, 23]. Although achieving these breakthroughs, the understanding of intrinsic microwave absorption, affected by the surface chemistry, is still virgin.

In this work, we report on the microwave absorption properties of three kinds of multi-walled carbon nanotube (MWCNT), namely pristine MWCNT (MWCNT-P), hydroxyl-containing MWCNT (MWCNT-OH) and carboxyl-containing MWCNT (MWCNT-COOH). Experimental data reveal that the absorption efficiencies of MWCNT-P, MWCNT-OH and MWCNT-COOH are > 33%, > 50% and > 45% at 8–18 GHz, respectively. With further experimental characterization, it is found that the atomic symmetry of surface structure for carbon nanotubes has been broken by the surface functional groups. And it leads to the differences of electric conductivity and dielectric loss capacity. The proper electromagnetic impedance matching emerged with a synergistic effect of permeability and permittivity, resulting from the decreasing electric conductivity. Moreover, an appropriate balance between reflection capacity and electromagnetic conversion capacity is observed, due to the accordance between reflection coefficient and dielectric loss.

Experiments

Electromagnetic measurements

The MWCNT-P, MWCNT-OH and MWCNT-COOH were purchased from Beijing DK Nano Technology Corporation, China, with an average length of 10–30 μm, dimensions of < 8 nm and purity of > 98%. The three kinds of MWCNT were mixed with paraffin at a mass ratio of 1:2 and then heated together at a constant temperature of 60 °C. Subsequently, the mixture was moved into a special model. And a ring sample, with thickness of 3 mm and inside and outside diameters of 3 mm and 7 mm, was obtained. The electromagnetic parameters were measured at 2–18 GHz by using a Keysight N5222A vector network analyzer with a sweep oscillator and an *S*-parameter test set. The electromagnetic wave reflection (*R*), transmission (*T*) and absorption (*A*) through the composites can be described directly by the S parameters as expressed by Eqs. (1)–(3) [24], which can directly indicate the microwave absorption efficiency.

$$R = |S_{11}|^2 \tag{1}$$

$$T = |S_{21}|^2 \tag{2}$$

$$A = 1 - R - T = 1 - |S_{11}|^2 - |S_{21}|^2. \tag{3}$$

It is noted that the S_{11} and S_{21} values in dB should be transformed to the reflection coefficient and the transmission coefficient using $S_{ij}(dB) = 20\lg|S_{ij}|$ (i,j = 1,2.), respectively.

Microstructure characterization

Scanning electron microscope (SEM) images were obtained using JEOL JSM-7001F field emission scanning electron microscope at an accelerating voltage at 15 kV. X-ray photoelectron spectroscopy (XPS, Thermal Scientific K Alpha) was performed with the Phoibos 100 spectrometer. Raman spectra of the three kinds of MWCNT were recorded on a Renishaw 1000 Raman spectrometer at the wavelength of the Raman laser of 532 nm.

Results and discussion

Microstructure characterizations

The microstructures of MWCNT-P, MWCNT-OH and MWCNT-COOH were initially characterized using a scanning electron microscope (SEM) and are presented in Fig. 1. SEM images shown in Fig. 1a–c confirm similar microstructure for the three kinds of MWCNT. These images also show that the three kinds of MWCNT remained intact with minimal visible tube damage and have basically the same size with an average length of 10–30 μm and a dimension range of ~ 8 nm. Furthermore, the dispersion of the three kinds of MWCNT in paraffin is shown in Fig. 2. SEM images shown in Fig. 2a–f prove that the three kinds of MWCNT can be uniformly dispersed in paraffin matrix.

The chemical composition of MWCNT was analyzed by using the X-ray photoelectron spectroscopy (XPS), and the results are shown in Figs. 3 and 4. The quantitative data of the three kinds of MWCNT are listed in Table 1. It can be seen that all the three kinds of MWCNT contain C and O. Besides C and O, a little

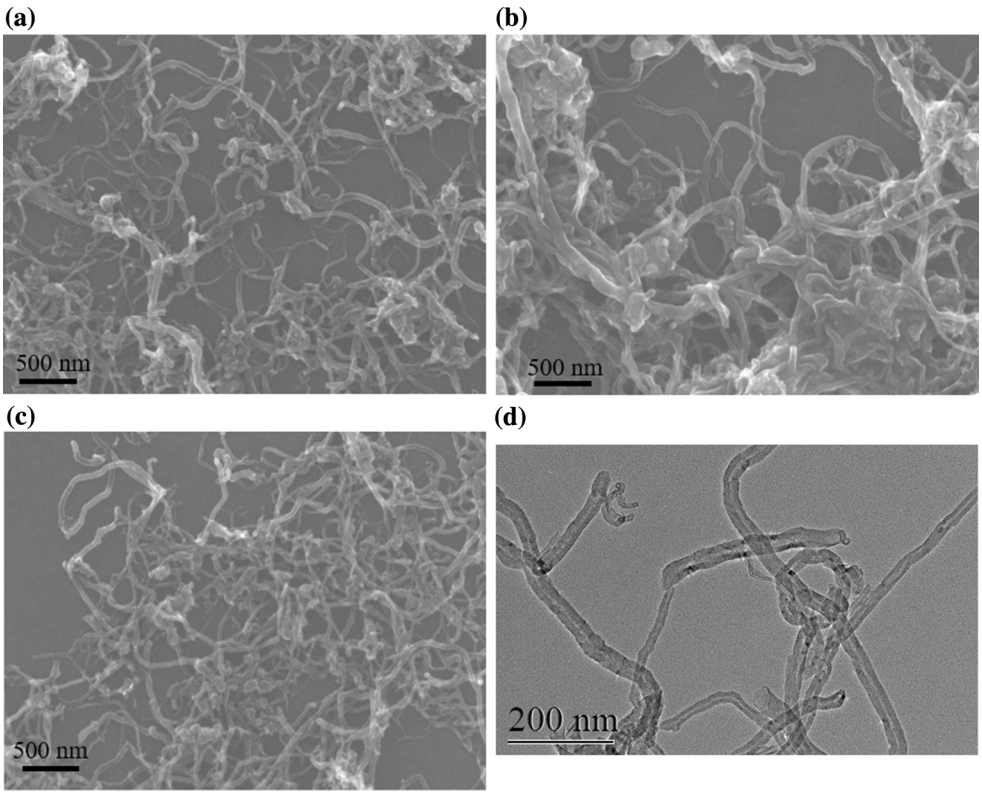

Figure 1 Microstructures. **a**–**c** SEM images of MWCNT-P, MWCNT-OH and MWCNT-COOH; **d** TEM image of MWCNT-OH.

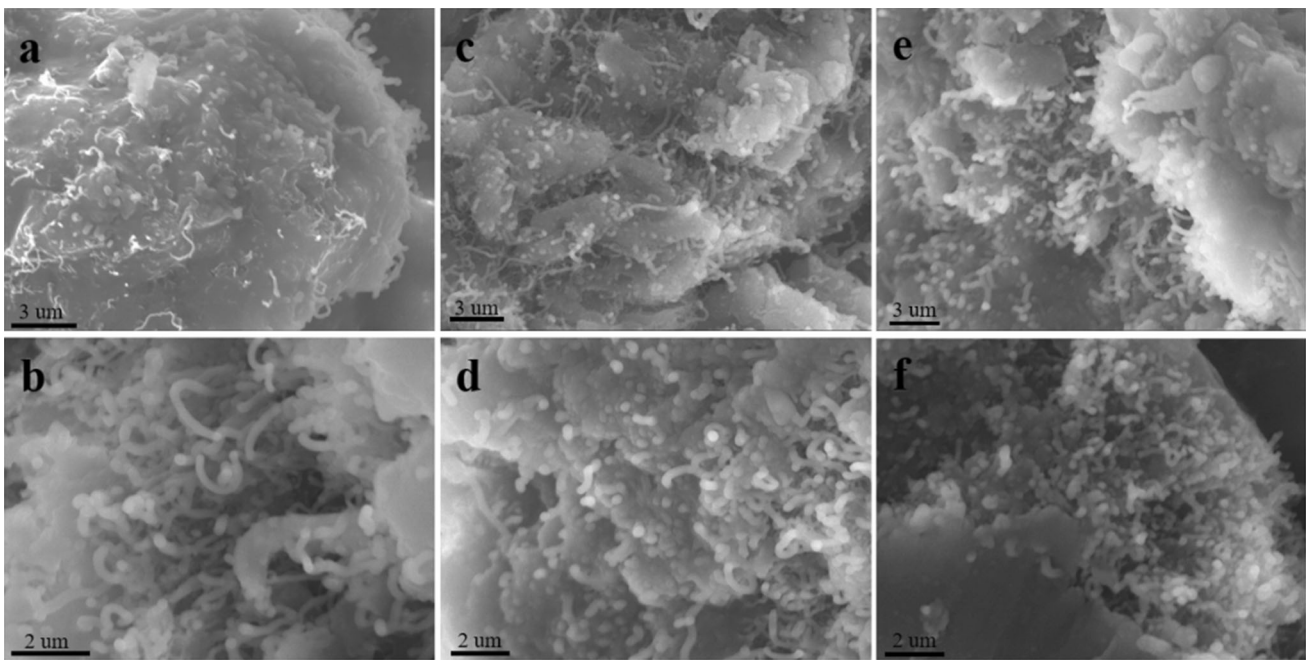

Figure 2 Dispersion of the three kinds of MWCNT in paraffin matrix. **a**, **b** SEM images of MWCNT-P; **c**, **d** SEM images of MWCNT-OH; **e**, **f** SEM images of MWCNT-COOH.

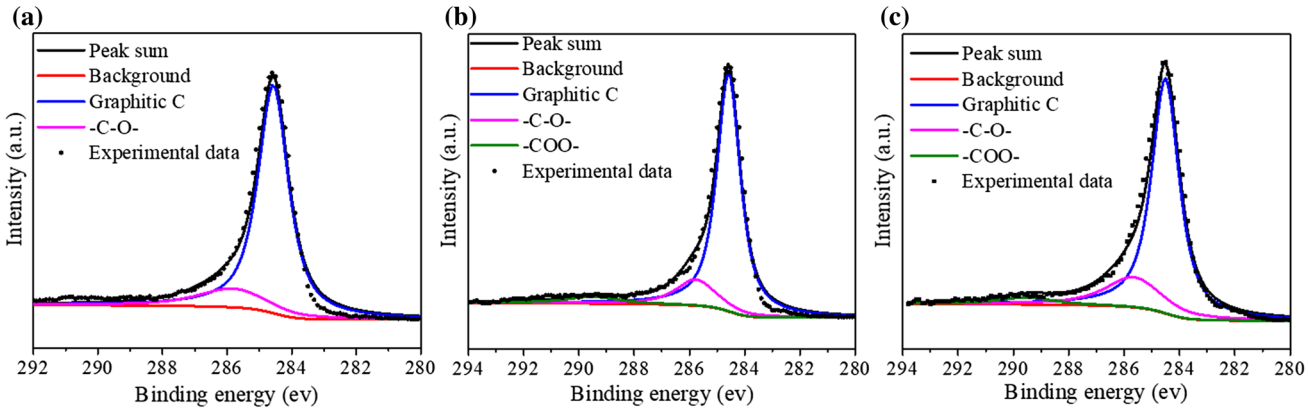

Figure 3 X-ray photoelectron spectroscopy analyses. **a**–**c** XPS spectra of C_{1s} characteristic peaks of MWCNT-P, MWCNT-OH and MWCNT-COOH.

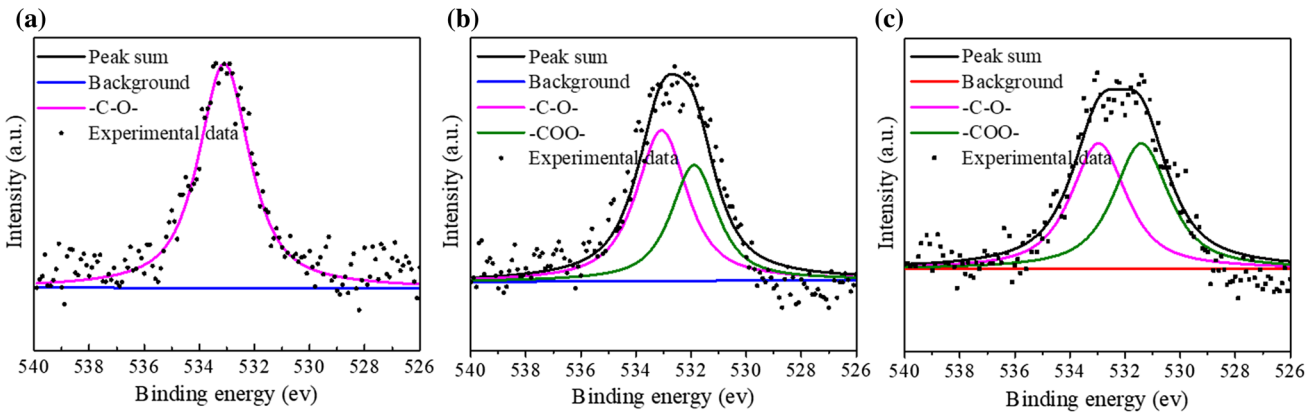

Figure 4 X-ray photoelectron spectroscopy analyses. **a**–**c** XPS spectra of O_{1s} characteristic peaks of MWCNT-P, MWCNT-OH and MWCNT-COOH.

content of N can be also observed from MWCNT-OH and MWCNT-COOH. Furthermore, carbon is the main component for the three kinds of MWCNT and the content of it decreases in the order of MWCNT-P, MWCNT-OH and MWCNT-COOH. Consequently, the content of oxygen increases with the same order. These observations indicate that MWCNT-COOH contains the largest amount of oxygen-containing functional groups among the three kinds of MWCNT.

The XPS spectra in the C1s region are presented in Fig. 3, analyzing the binding states. Although there are many existing states of oxygen in the MWCNT, it can be mainly divided into two sub-peaks of –C–O– and –COO– at 285.8 eV and 289.1 eV [25–30]. The C1s peak in all the XPS spectra shows a dominant peak structure at a binding energy of 284.4 eV, which corresponds to the graphitic carbons. In addition to the carbon in the skeleton of MWCNT, the functional group –C–O– can also be derived in the MWCNT-P, as shown in Fig. 3a. Two peaks of –C–O– and –COO– can be observed from the XPS spectra in the C1s region of MWCNT-OH and MWCNT-COOH, as shown in Fig. 3b, c. It can be concluded from Fig. 3 that the content of functional groups in the MWCNT-COOH is the highest among all MWCNTs and the content of carboxyl group in the MWCNT-COOH is much higher than that in the MWCNT-OH.

As the strength of graphitic carbon peak is significantly higher than other peaks, the information of functional groups containing carbon and oxygen

Table 1 Atomic concentrations of C, O and N in the three kinds of MWCNT

Element	MWCNT-P (at.%)	MWCNT-OH (at.%)	MWCNT-COOH (at.%)
C	96.8	92.4	92.0
O	3.2	5.0	6.7
N	/	2.6	1.3

cannot be clearly obtained in the C1 s region. So the XPS spectra in the O1s region were investigated to provide supplementary information shown in Fig. 4. The width of O1s peaks of the three kinds of MWCNT increases in the following order: MWCNT-P, MWCNT-OH and MWCNT-COOH. Obviously, the spectrum of MWCNT-P displays only one peak at 533.0 eV, which indicates the existence of –C–O–, while the spectrum of MWCNT-OH and MWCNT-COOH displays two peaks corresponding to hydroxyl (C–OH) and carboxylic (COOH) [31–33]. Moreover, the difference between the relative contents of –C–O– and –COO– can be clearly distinguished between MWCNT-OH and MWCNT-COOH. Compared with MWCNT-COOH, MWCNT-OH contains more –C–O– instead of –COO–. These further confirm the results derived from Fig. 3.

As a very valuable tool to characterize carbon-based nanostructures, the Raman spectra of MWCNT-P, MWCNT-OH and MWCNT-COOH taken at the wavelength of the Raman laser (λ) of 532 nm are shown in Fig. 5 (a). For all samples, it presents three main peaks, namely *D* peak at $\sim$ 1344 cm^{-1}, G peak at $\sim$ 1571 cm^{-1} and 2*D* peak at $\sim$ 2677 cm^{-1}. The *D* peak corresponds to the first-order scattering process of sp2 carbons. And it is generally activated by the existence of vacancies, surface functional groups, boundaries and other defects. The G peak derives from the in-plane tangential stretching of –C–C– in graphitic shells, and the 2*D* peak is the second order of mode of the *D* peak [34, 35]. It is found that the ratio of the intensities of *D* peak and G peak (I_D/I_G) increases in the order of MWCNT-P (0.77), MWCNT-OH (0.79) and MWCNT-COOH (0.94). Hereafter, the average distance between two defect sites (L_D) can be estimated by Eq. (4) [36, 37].

$$L_D^2 = (1.8 \pm 0.5) \times 10^{-9} \times \lambda^4 \times (I_D/I_G)^{-1}. \quad (4)$$

The obtained defect distances are 13.68 nm, 13.51 nm and 12.38 nm for MWCNT-P, MWCNT-OH and MWCNT-COOH, respectively. Therefore, the concentration of defect sites increases in the order of MWCNT-P, MWCNT-OH and MWCNT-COOH. Moreover, Fig. 5b shows the relationship between the graphite domain size (L_a) and the ration of I_{2D}/I_G. And the L_a can be evaluated by Eq. (5) [38, 39]. It can be found that the L_a values decrease in the order of MWCNT-P, MWCNT-OH and MWCNT-COOH. It is therefore indicated that the incorporation of surface functional groups could break the atomic-scale structural symmetry of carbon nanotubes.

$$L_a = \left(2.4 \times 10^{-10}\right) \times \lambda^4 \times (I_D/I_G)^{-1}. \quad (5)$$

Electromagnetic properties

The electromagnetic response characteristics of the three kinds of MWCNT were evaluated at 2–18 GHz by a vector network analyzer. As shown in Fig. 6, the scattering parameters (*S* parameters) of the three kinds of MWCNT mixed with paraffin in mass ratio

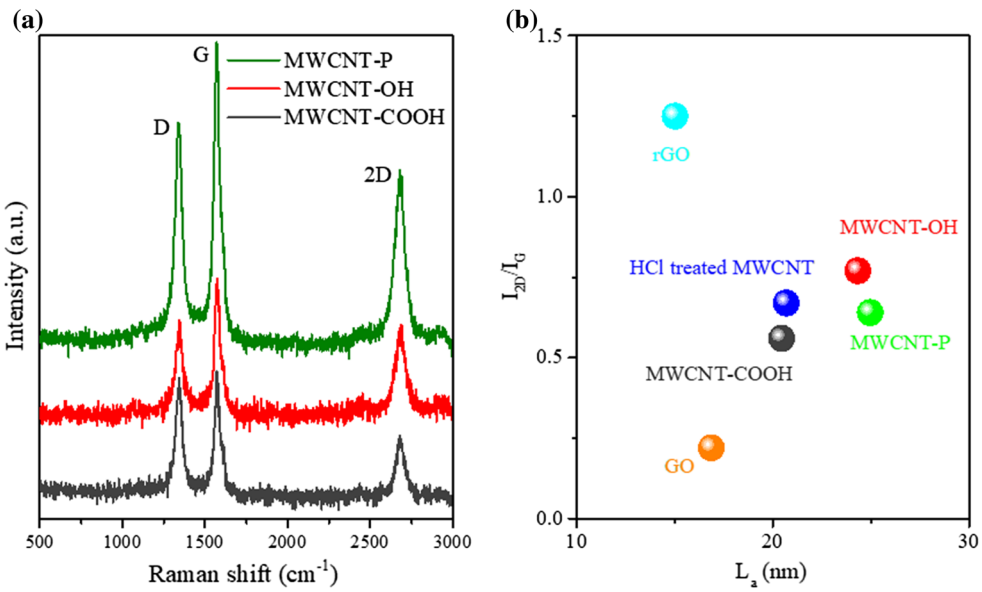

Figure 5 Raman spectroscopy of MWCNT-P, MWCNT-OH and MWCNT-COOH. **a** Raman spectroscopy of D, G and 2D bands of the three kinds of MWCNT; **b** evolution of the crystalline domains L_a versus I_{2D}/I_G for MWCNT-P, MWCNT-OH, MWCNT-COOH, HCl-treated MWCNT, GO and rGO, respectively.

of 1:2 depend on the frequency and present the same trend as frequency changes, all decreasing along with the increasing frequency. To further investigate the effect of functional groups containing carbon and oxygen on electromagnetic properties, the S parameters of the three kinds of MWCNT are compared, in view of these results above. It is found that the S_{11} increases in the order of MWCNT-OH, MWCNT-COOH and MWCNT-P, while the S_{21} increases in the reverse order, resulting in the highest absorption performance obtained by MWCNT-OH. The absorption efficiencies of MWCNT-P, MWCNT-OH and MWCNT-COOH are $> 33\%$, $> 50\%$ and $> 45\%$ at 8–18 GHz, respectively.

In order to understand the mechanism of the microwave absorption at different functional groups, the dependence of the complex permittivity and permeability on frequency was investigated. Figure 7a, b shows the dependence of the real part (ε') and imaginary part (ε'') of complex permittivity on the frequency. For all the samples, the values of ε' decrease over 2–18 GHz with a rapid speed from 2 to 8 GHz and a slow speed from 8 to 18 GHz. Obviously, the ε' values decrease in the order of MWCNT-P, MWCNT-COOH and MWCNT-OH at 2–8 GHz and MWCNT-COOH, MWCNT-P and MWCNT-OH at 8–18 GHz. For all samples, the ε'' values decrease with the increasing frequency at 2–18 GHz and the ε'' values of MWCNT-OH and MWCNT-COOH are much lower than the value of MWCNT-P. As a dielectric material, the real part (μ') and imaginary part (μ'') of complex permeability of the three kinds of MWCNT are reasonably thought to be 1 and 0, respectively. The ε' values correspond to the storage capacity of electric energy. And a ε' value close to μ' generates a balance between permittivity and permeability, leading to an increased absorption performance. In order to further understand the wax on the electromagnetic properties at different functional groups, the dielectric loss ($\tan\delta_\varepsilon$) was calculated by Eq. (6) [40].

$$\tan\delta_\varepsilon = \frac{\varepsilon''}{\varepsilon'}. \tag{6}$$

The dielectric loss is a critical factor to evaluate the electromagnetic performance of materials. With higher $\tan\delta_\varepsilon$ value, more electromagnetic energy can be transformed into other forms of energy, mainly thermal energy. The dielectric loss ($\tan\delta_\varepsilon$) was investigated, and the results are shown in Fig. 7c. The values decreased in the order of MWCNT-P, MWCNT-OH and MWCNT-COOH, indicating a decreased conversion capacity of electromagnetic energy.

It should be noted that although the dielectric loss of MWCNT-OH is not the highest, it presented the best microwave absorption performance, which may be resulted from the balance between the two key factors. For MWCNT-P with high electromagnetic conversion capacity, the energy has already been reflected back before converted due to the high reflection coefficient, resulting in a low absorption. For MWCNT-COOH, the high reflection coefficient and low electromagnetic energy conversion lead to a low absorption performance. For MWCNT-OH, a balance emerged between reflection coefficient and electromagnetic conversion, and the best absorption performance was obtained as a result. Furthermore, it is found that the volume of nanotubes is basically the same from the direct statistic observation based on

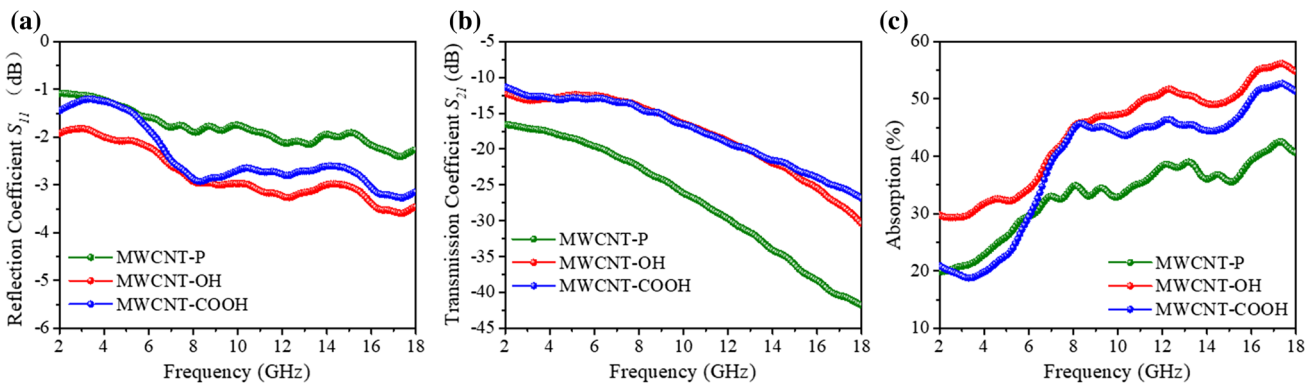

Figure 6 Scattering parameters of MWCNT-P, MWCNT-OH and MWCNT-COOH mixed with paraffin in mass ratio of 1:2. **a**–**c** the reflection coefficient (S_{11}), transmission coefficient (S_{21}) and absorption values.

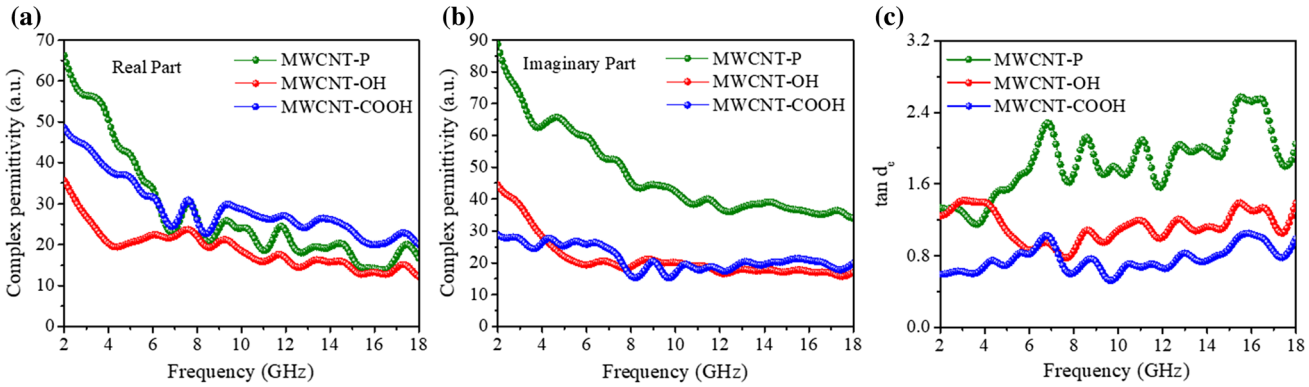

Figure 7 Relative complex permittivity and permeability of MWCNT-P, MWCNT-OH and MWCNT-COOH mixed with paraffin in mass ratio of 1:2. **a** and **b** the real part and imaginary part of the relative complex permittivity; **c** the dielectric loss and magnetic loss.

the SEM images. And with the analysis of Raman, it can be concluded that the introduction of surface functional groups increases the concentration of defect sites and decreases the graphitic domain size, leading to the breaking of the micro-symmetry of carbon nanotubes. Therefore, it can be indicated that the damage degree leads to higher reflection coefficient and lower electromagnetic energy conversion of MWCNT-COOH than those of MWCNT-OH.

Two key factors should be satisfied for a good electromagnetic absorber. One is the impedance match, requiring the equality of the electromagnetic parameters. The decreases in ε' and ε'' would inevitably lead to the increase in impedance match when μ' and μ'' are 1 and 0, respectively. As shown in Fig. 7, the MWCNT-OH displays the lowest ε' and lower ε'', thus leading to the best impedance match. The other one is the attenuation constant, which can be calculated by Eq. (7) [41].

$$\alpha = \frac{\sqrt{2}\pi f}{c} \times \sqrt{(\mu''\varepsilon'' - \mu'\varepsilon') + \sqrt{(\mu''\varepsilon'' - \mu'\varepsilon')^2 + (\varepsilon'\mu'' + \varepsilon''\mu')^2}}. \quad (7)$$

As shown in Fig. 8, the dependence of α on the frequency for the MWCNT-OH has the maximum α among all samples in the whole frequency range, indicating the excellent attenuation capacity. From Eq. (7), it can be noticed that higher value of ε'' and lower value of ε' would result in higher α. The MWCNT-OH displays the lowest ε' and higher ε'', thus leading to the best microwave absorption performance, ascribed to its high dielectric loss capacity.

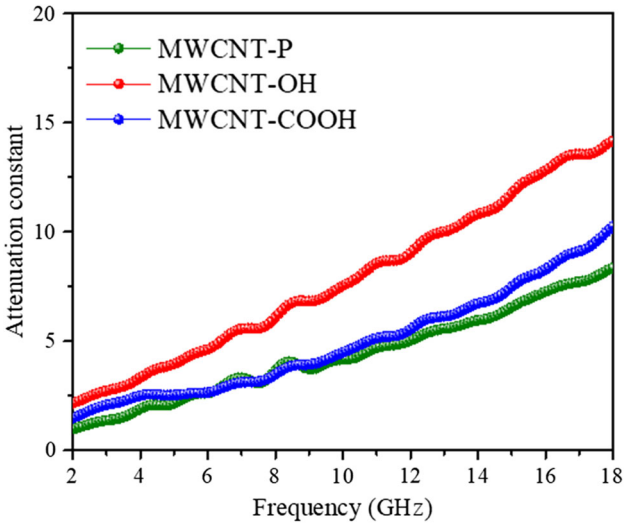

Figure 8 Frequency dependence of the attenuation constant of the three kinds of MWCNT.

Moreover, the *S* parameters of the three kinds of MWCNT mixed with paraffin in mass ratio of 1:4 are compared in Fig. 9. It can be seen that the trends of *S* parameters are basically the same as mentioned above. And the absorption efficiencies of MWCNT-P, MWCNT-OH and MWCNT-COOH are 53%, 63% and 56% at 14–18 GHz, respectively.

The electromagnetic properties of the three kinds of MWCNT mixed with paraffin at different mass ratios are presented in Fig. 10. It can be seen that with the reduced filling ratio of MWCNT, the real part and imaginary part of complex permittivity of all the three kinds of MWCNT decreased, showing that the electromagnetic characteristics are only originated from the dielectric nature of MWCNT. Thus, the electromagnetic properties of the three kinds of

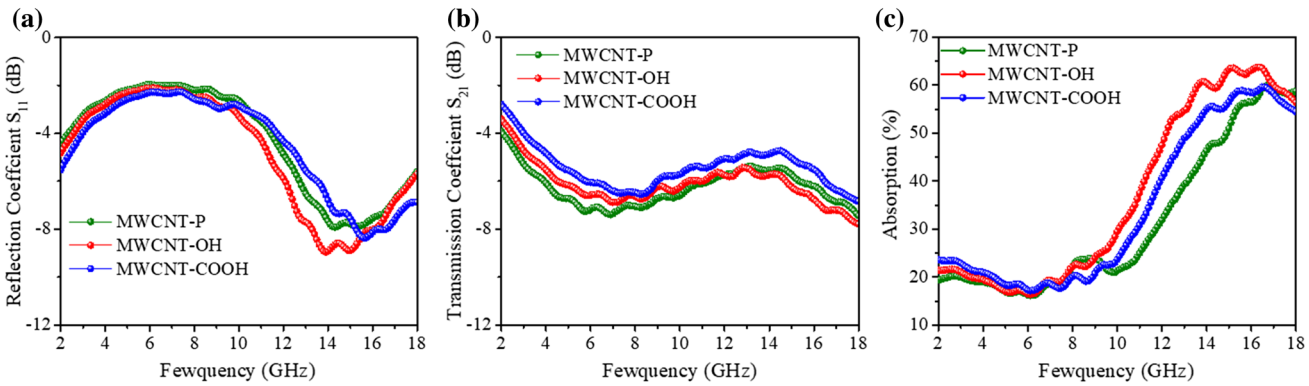

Figure 9 Scattering parameters of MWCNT-P, MWCNT-OH and MWCNT-COOH mixed with paraffin in mass ratio of 1:4. **a**–**c** the reflection coefficient (S_{11}), transmission coefficient (S_{21}) and absorption values.

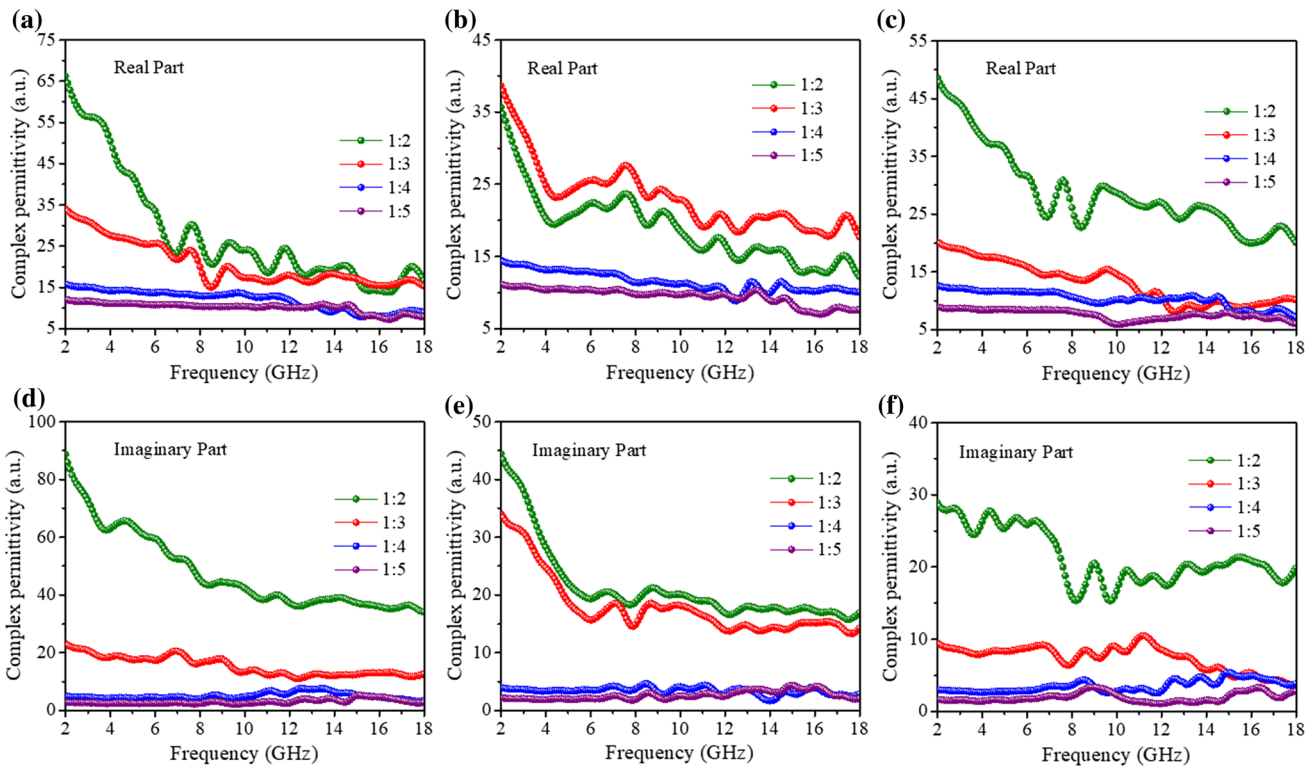

Figure 10 Relative complex permittivity of MWCNT-P, MWCNT-OH and MWCNT-COOH mixed with paraffin in different mass ratios. **a**–**c** the real part of the relative complex permittivity of MWCNT-P, MWCNT-OH and MWCNT-COOH; **d**–**f** the imaginary part of the relative complex permeability of MWCNT-P, MWCNT-OH and MWCNT-COOH.

MWCNT mixed with paraffin only in mass ratio of 1:2 were specifically discussed.

Conclusion

To conclude, the microwave absorption properties of the three kinds of MWCNT, namely MWCNT-P, MWCNT-OH and MWCNT-COOH, have been presented. It is found that the absorption properties of MWCNT depend on the surface functional groups. The absorption efficiencies of MWCNT-P, MWCNT-OH and MWCNT-COOH at 8–18 GHz are $> 33\%$, $> 50\%$ and $> 45\%$, respectively. Compared with MWCNT-P, an absorption efficiency of 17% of MWCNT-OH is significantly enhanced. The surface functional groups containing carbon and oxygen break the atomic symmetry of surface structure of

carbon nanotubes, leading to the differences of electric conductivity and dielectric loss capacity. On the one hand, the synergistic effect of complex permeability and permittivity leads to a proper electromagnetic impedance matching. On the other hand, the accordance between the reflection coefficient and dielectric loss brings about an appropriate balance between reflection capacity and electromagnetic conversion capacity. Eventually, the tunability of absorption capacity is observed. The present study provides an insight into the structural origin of microwave absorption and has important significance to design microwave absorption materials by chemical surface engineering.

Acknowledgements

The authors gratefully acknowledge the National Natural Science Foundation of China (U1704253), (51471045), and the Fundamental Research Funds for the Central Universities (N160208001).

Compliance with ethical standards

Conflicts of interest The authors declare that they have no conflict of interest.

References

[1] Sharma BK, Khare N, Sharma R, Dhawan SK, Vankar VD, Gupta HC (2009) Dielectric behavior of polyaniline-CNTs composite in microwave region. Compos Sci Technol 69:1923–1935

[2] Min DD, Zhou WC, Qing YC, Luo F, Zhu DM (2017) Greatly enhanced microwave absorption properties of high oriented flake carbonyl iron/epoxy resin composites under applied magnetic field. J Mater Sci 52:2373–2383. https://doi.org/10.1007/s10853-016-0532-1

[3] Li W, Wu TL, Wang W, Guan JG, Zhai PC (2014) Integrating non-planar metamaterials with magnetic absorbing materials to yield ultra-broadband microwave hybrid absorbers. Appl Phys Lett 104:022903

[4] Zhang Y, Huang Y, Zhang TF, Chang HC, Xiao PS, Chen HH (2015) Broadband and tunable high-performance microwave absorption of an ultralight and highly compressible graphene foam. Adv Mater 27:2049–2053

[5] Zhang XF, Dong XL, Huang H, Liu YY, Wang WN, Zhu XG (2006) Microwave absorption properties of the carbon-coated nickel nanocapsules. Appl Phys Lett 89:053115

[6] Wang ZH, Wang JY, Li YX, Liu RG, Zhang YH, Zhao XN (2018) Multi-interfacial Co@CoN$_x$@C(N) nanocapsules with nitrogen substitutions in graphitic shells for improving microwave absorption properties. J Alloy Compd 736:51–56

[7] Liu XG, Cui CY, Yu JY, Sun YP, Xia AL (2018) Ag3PO4 sub-microcubic/SrFe12O19 hexagon nanoflake heterostructure for broadband electromagnetic absorber at GHz frequency. Mater Lett 225:1–4

[8] Zou Z, Xuan AG, Yan ZG, Wu YX, Li N (2010) Preparation of Fe3O4 particles from copper/iron ore cinder and their microwave absorption properties. Chem Eng Sci 65:160–164

[9] Kittel C (1948) On the theory of ferromagnetic resonance absorption. Phys Rev 73:155–161

[10] Long C, Xu BC, Han CZ, Chen ZH, Guan JG (2017) Flaky core-shell particles of iron@iron oxides for broadband microwave absorbers in S and C bands. J Alloy Compd 709:735–741

[11] Ting TH, Wu KH (2010) Synthesis, characterization of polyaniline/$BaFe_{12}O_{19}$ composites with microwave-absorbing properties. J Magn Magn Mater 322:2160–2166

[12] Namai A, Sakurai S, Nakajima M, Suemoto T, Matsumoto K, Goto M (2009) Synthesis of an electromagnetic wave absorber for high-speed wireless communication. J Am Chem Soc 131:1170–1173

[13] Zhang XF, Rao Y, Guo JJ, Qin GW (2016) Multiple-phase carbon-coated $FeSn_2$/Sn nanocomposites for high-frequency microwave absorption. Carbon 96:972–979

[14] Liu XG, Ran SL, Yu JY, Sun YP (2018) Multiscale assembly of Fe_2B porous microspheres for large magnetic losses at gigahertz. J Alloy Compd 765:943–950

[15] Kresse G, Joubert D (1999) Form ultrasoft pseudopotentials to the projector augmented-wave method. Phys Rev B 59:1758–1775

[16] Park KY, Lee SE, Kim CG, Han JH (2006) Fabrication and electromagnetic characteristics of electromagnetic wave absorbing sandwich structures. Compos Sci Technol 66:576–584

[17] Kresse G, Hafner J (1994) Ab initio molecular-dynamics simulation of the liquid-metal-amorphous-semiconductor transition in germanium. Phys Rev B 49:14251–14269

[18] Lijima S (1991) Helical microtubules of graphitic carbon. Nature 354:56–58

[19] Ajayan PM (1999) Nanotubes from carbon. Chem Rev 99:1787–1800

[20] Sinnott BS (2002) Chemical functionalization of carbon nanotubes. J Nanosci Nanotechnol 2:113–123

[21] Luo QM, Wei PR, Huang QW, Gurkan B, Pentzer EB (2018) Carbon capsules of ionic liquid for enhanced performance of electrochemical double-layer capacitors. Appl Mater Interfaces 10:16707–16714

[22] Che RC, Peng LM, Duan XF, Chen Q, Liang XL (2004) Microwave absorption enhancement and complex permittivity and permeability of Fe encapsulated within carbon nanotubes. Adv Mater 16:401–405

[23] Liu G, Wang LY, Chen GM, Hua SC, Ge CQ, Zhang H (2012) Enhanced electromagnetic absorption properties of carbon nanotubes and zinc oxide whisker microwave absorber. J Alloy Compd 15:183–188

[24] Brosseau C, Dong WN, Mdarhri A (2008) Influence of uniaxial tension on the microwave absorption properties of filled polymers. J Appl Phys 104:070907

[25] Bi HQ, Li YH, Liu SF, Guo PZ, Wei ZB, Lv CX (2012) Carbon-nanotube-modified glassy carbon electrode for simultaneous determination of dopamine, ascorbic acid and uric acid: the effect of functional groups. Sens Actuators B Chem 172:1132–1140

[26] Xing YC, Li L, Chusuei CC, Hull RV (2005) Sonochemical oxidation of multiwalled carbon nanotubes. Langmuir 21:4185–4190

[27] Li P, Liu HL, Yang J, Sun DM, Chen Y, Zhou YM (2013) A ruthenium(III) phosphonate complex on polyallylamine functionalized carbon nanotube multilayer films: self-assembly, direct electrochemistry, and electrocatalysis. J Mater Chem B 2:102–109

[28] Roy S, Sahoo NG, Cheng HKF, Das CK, Chan SH, Li L (2011) Molecular interaction and properties of poly(ether ether ketone)/liquid crystalline polymer blends incorporated with functionalized carbon nanotubes. J Nanosci Nanotechnol 11:10408–10416

[29] Okpalugo TIT, Papakonstantinou P, Murphy H, Mclaughlin J, Brown NMD (2005) High resolution XPS characterization of chemical functionalised MWCNTs and SWCNTs. Carbon 43:153–161

[30] Xue SM, Xu ZL, Tang YJ, Ji CH (1994) Polypiperazine-amide nanofiltration membrane modified by different functionalized multiwalled carbon nanotubes (MWCNTs). ACS Appl Mater Interfaces 8:19135–19144

[31] Datsyuk V, Kalyva M, Papagelis K, Parthrnios J, Tasis D, Siokou A (2008) Chemical oxidation of multiwalled carbon nanotubes. Carbon 46:833–840

[32] Martinez MT, Callejas MA, Benito AM, Cochet M, Seeger T, Anson A (2003) Sensitivity of single wall carbon nanotubes to oxidative processing: structural modification, intercalation and functionalization. Carbon 41:2247–2256

[33] Hontoria-Lucas C, Lopez-Peinado AJ, Lopez-Gonzalez JD, Rojas-Cervantes ML, Martin-Aranda RM (1995) Study of oxygen-containing groups in a series of graphite oxides: physical and chemical characterization. Carbon 33:1585–1592

[34] Datsyuk V, Kalyva M, Papagelis K, Parthenios J, Tasis D, Siokou A (2008) Chemical oxidation of multiwalled carbon nanotubes. Carbon 46:833–840

[35] Martinez MT, Callejas MA, Benito AM, Cochet M, Seeger T, Anson A (2003) Sensitivity of single wall carbon nanotubes to oxidative processing: structural modification, intercalation and functionalization. Carbon 41:2247–2256

[36] Dresselhaus MS, Jorio A, Hofmann M, Dresselhaus G, Saito R (2010) Perspective on carbon nanotubes and grapheme Raman spectroscopy. Nano Lett 10:751–756

[37] Cancado LG, Jorio A, Ferreira EHM, Stavale F, Achete CA, Capaz RB (2011) Quantifying defects in graphene via raman spectroscopy at different excitation energies. Nano Lett 11:3190–3196

[38] Cancado LG, Takai K, Enoki T, Endo M, Kim YA, Mizusaki H (2006) General equation for the determination of the crystallite size La of nanographite by raman spectroscopy. Appl Phys Lett 88:163106

[39] Ferrari AC, Meyer JC, Scardaci V, Casiraghi C, Lazzeri M, Mauri F (2006) Raman spectrum of graphene and graphene layers. Phys Rev Lett 97:187401

[40] Sun H, Che RC, You X, Jiang YS, Yang ZB, Deng J (2014) Cross-stacking aligned carbon-nanotube films to tune microwave absorption frequencies and increase absorption intensities. Adv Mater 26:8120–8125

[41] Lu B, Huang H, Dong XL, Zhang XF, Lei JP, Sun JP (2008) Influence of alloy components on electromagnetic characteristics of core/shell-type Fe-Ni nanoparticles. J Appl Phys 104:114313